CrossMark

ORIGINAL ARTICLE

Application of maghemite nanoparticles as sorbents for the removal of Cu(II), Mn(II) and U(VI) ions from aqueous solution in acid mine drainage conditions

Anita Etale · Hlanganani Tutu · Deanne C. Drake

Abstract The adsorptive removal of Cu(II), Mn(II) and U(VI) by maghemite nanoparticles (NPs) was investigated under acid mine drainage (AMD) conditions to assess NP potential for remediating AMD-contaminated water. The effects of time, NP and metal concentration, as well as manganese and sulphate ions were quantified at pH 3. Adsorption of all three ions was rapid, and equilibrium was attained in 5 min or less. 56 % of Cu, 53 % of Mn and 49 % of U were adsorbed. In addition, adsorption efficiencies were enhanced by ≥ 10 % in the presence of manganese and sulphate ions, although Cu sorption was reduced in 1:2 Cu-to-Mn solutions. Adsorption also increased with pH: 86 % Cu, 62 % Mn and 77 % U were removed from solution at pH 9 and increasing initial metal concentrations. Increasing NP concentrations did not, however, always increase metal removal. Kinetics data were best described by a pseudo-second-order model, implying chemisorption, while isotherm data were better fitted by the Freundlich model. Metal removal by NPs was then tested in AMD-contaminated surface and ground water. Removal efficiencies of up to 46 % for Cu and 54 % for Mn in surface water and 8 % for Cu and 50 % for Mn in ground water were achieved, confirming that maghemite NPs can be applied for the removal of these ions from AMD-contaminated waters. Notably, whereas sulphates may increase adsorption efficiencies, high Mn concentrations in AMD will likely inhibit Cu sorption.

Introduction

The contamination of water bodies by metal and radionuclide ions is a major unintended consequence of mining in many regions of the world. In South Africa, mining of base and precious metals has taken place for more than a century and contributed enormously to the growth of the economy. It has also, however, resulted in significant contamination of surface and groundwater by acid mine drainage (AMD) and a suite of metal and radionuclide ions (Naicker et al. 2003; Tutu et al. 2008; Winde 2010). This contamination is a major concern especially in light of the health risks and negative impacts on ecosystems posed by exposure to excessive metal concentrations (WHO 2011). Cu, for example, is toxic to some algae at sub-ppm (parts per million/mg L^{-1}) concentrations (Franklin et al. 2000); and U has been linked to renal failure and certain cancers in humans (Toens et al. 1998; WHO 2011). Mn, although less toxic, lends undesirable qualities like poor taste and staining to potable water. The World Health Organization (WHO) drinking water standards stipulate upper limits of 2 mg L^{-1}, 0.4 mg L^{-1} and 30 µg L^{-1} for Cu, Mn and U, respectively (WHO 2011). Yet concentrations as high as 7 mg L^{-1} for Cu, 129 mg L^{-1} for Mn and 2.6 mg L^{-1} for U have been reported for ground and surface waters sometimes used for potable purposes (Naicker et al. 2003; Tutu et al. 2008; Winde 2010; Saad et al. 2013). The removal of these ions from AMD-contaminated waters is

A. Etale (✉) · D. C. Drake
School of Animal Plant and Environmental Sciences, University of the Witwatersrand, Private Bag X3, WITS, 2050 Johannesburg, South Africa
e-mail: aetale@gmail.com

H. Tutu
Molecular Sciences Institute, School of Chemistry, University of the Witwatersrand, Private Bag X3, WITS, 2050 Johannesburg, South Africa

KACST مدينة الملك عبدالعزيز للعلوم والتقنية

Springer

therefore necessary to reduce negative effects to humans, aquatic organisms and ecosystems. Remediation is also necessary in light of the scarcity of water as a resource and the growing water scarcity and the increasing pressures on this resource by increasing human population and per capita rates of water use.

A number of techniques exist for the removal of metal and radionuclide ions from wastewater, e.g., ion exchange, reverse osmosis, phytoremediation, electrodialysis and chemical precipitation (Kurniawan et al. 2006). These, however, suffer from limitations like low adsorbent capacities, fouling, high maintenance costs, slow uptake rates and production of large quantities of secondary wastes. Adsorption offers an alternative that is free from some of these limitations and as such, has been extensively studied. Among the many adsorbents investigated, e.g., activated carbon, zeolites, polymers, zero-valent iron and agricultural wastes (Fu and Wang 2011), nanoparticles (NPs) have attracted considerable interest due to the special properties of materials at the nanoscale (1–100 nm). NPs are more reactive than larger materials and offer larger sorption surface areas, thus allowing for faster and more efficient adsorption (Waychunas and Zhang 2008).

NPs of various materials such as carbon (e.g., carbon nanotubes), metals (e.g., zero-valent iron) and metal oxides (e.g., titania, iron oxides) have been investigated for the adsorptive removal of metal ions from water (see review by Khajeh et al. 2013). Of the iron oxides, maghemite nanomaterials have shown good efficiency for the removal of ions including As(V) (Tuutijärvi et al. 2009), Mo(VI) (Afkhami and Norooz-Asl 2009), Cr(VI) (Jiang et al. 2013), Cu, Zn, Pb (Roy and Bhattacharya 2012), Se (Jordan et al. 2013) and U (Madrakian et al. 2011). Hu et al. (2006), for example, reported an adsorption capacity of 27.7 mg g^{-1} for Cu at pH 6.5 and 25.7 mg g^{-1} for Ni at pH 8.5. Less information is, however, available on the adsorptive removal of Mn from wastewater by NPs. Perhaps this is due to the lower toxicity of Mn in comparison to other elements. But concentrations in AMD easily surpass limits for drinking water and organism tolerance, hence the need for its removal.

A review of the literature revealed a paucity of information on metal removal by NPs in mine drainage conditions. The pH in AMD, for example, is often ≤3 and adsorption in such extreme pH is different from pH 6 at which many studies are conducted. Further, AMD contains additional ions such as manganese and sulphates that are likely to affect the adsorption efficiency of NPs and any remediation technology applied. Manganese and sulphates are abundant in mine drainage, being the products of pyrite (FeS$_2$) and MnS oxidation (Schemel et al. 2000). However, unlike ferric ions that are also abundant but precipitate at low pH, manganese persists in solution over a wide range

of pH and may therefore have an effect on adsorption of other cations. The successful treatment of AMD using NPs requires that these effects are quantified to improve the optimal functioning of remediation technologies.

We therefore designed a study to investigate the use of NPs for the adsorptive removal of metal ions common in AMD. Herein, we report on the findings of the application of maghemite for the removal of Cu(II), Mn(II) and U(VI) from simulated AMD. The effects of time, adsorbate concentrations, adsorbent concentrations as well as those of sulphate and manganese ions on adsorption of these three ions were investigated. We also quantified the adsorption process at pH 5, 7 and 9 to determine process efficiency in pH-amended systems.

Materials and methods

Materials

All metal salts used for this study were analytical grade. Cu(NO$_3$)$_2$·2.5·H$_2$O and Mn(NO$_3$)$_2$·H$_2$O were purchased from Sigma Aldrich (Germany). UO$_2$(NO$_3$)$_2$·6H$_2$O and Na$_2$SO$_4$ were from Ace Chemicals (South Africa), and maghemite NPs from Sigma Aldrich (Germany). Metal salt solutions and NP suspensions were prepared using deionised water. NP suspensions (3 mg L^{-1}) were prepared by 30-min sonication in a water bath (Branson 2500). Adjustments of solution pH were made prior to experiments using 0.01 M HNO$_3$ and 0.01 M NaOH.

Particle characterisation

The size and morphology of maghemite particles was determined using transmission electron microscopy (FEI Tecnai G^2 Spirit TEM) at an acceleration voltage of 120 kV. Particles (0.1 g) were suspended in 100-mL deionised water and sonicated in a water bath for 30 min. A drop of the suspension was then placed on a copper grid and left to dry for 20 min before analysis. The surface area of particles was determined by the Brunauer–Emmett–Teller (BET) method using a Micrometrics Tristar 3000 (Micrometrics Instruments, USA). NP crystallinity was determined by powder X-ray diffraction on a Bruker D8 diffractometer (Cu-Kα). The scanning range was 10°–90° (2θ) using a step size of 0.026° and step time of 37 s at room temperature (25 °C ± 2).

Adsorption studies

Adsorption was quantified in batch experiments using solutions of 14.99 mg L^{-1} Cu, 9.52 mg L^{-1} Mn and 42.18 mg L^{-1} U. Freshly sonicated NP suspensions (10 mL)

were contacted with 10-mL metal nitrate solutions in 50-mL polyethylene terephthalate (PET) jars. Experiments were run in triplicate, for 60 min, at ambient temperature (~ 25 °C) and unless otherwise stated, at pH 3.3 (± 0.2).

The effect of contact time was evaluated for durations ranging from 5 s to 60 min (5, 10, 15, 30, 45, 60, 300, 600, 900, 1,800, 2,700 and 3,600 s). The effects of Mn^{2+} (from $Mn(NO_3)_2 \cdot H_2O$) and SO_4^{2-} (from Na_2SO_4) were quantified for 1:1 and 1:2 molar ratios to the test ion. The effects of both additional ions were tested for Cu and U, but for Mn, only SO_4^{2-} effects were investigated. The effect of adsorbent concentration on adsorption efficiency was tested using 1, 3 and 10 mg L^{-1} maghemite concentrations while that of pH was tested at pH 3, 5, 7 and 9. Finally, adsorption isotherms were investigated for concentrations ranging from 14.99–136.4 mg L^{-1} for Cu, 9.52–104.6 mg L^{-1} for Mn and 4.46–464.2 mg L^{-1} for U.

At the end of experiments, mixtures were separated using Amicon ultracentrifugal filters (100 kDa molecular weight cut off; Millipore) and filtrates acidified with 3 mL 1 % nitric acid. Metal concentrations in filtrates were determined by Inductively Coupled Plasma-Optical Emission Spectrometry (ICP-OES; Spectro Instruments, Kleve, Germany). Adsorption at the various time intervals and at equilibrium was determined by mass-balance calculations.

The equilibrium adsorption capacities of NPs (q_e; mg g^{-1}) were calculated using Eq. 1. Adsorption efficiency was expressed as a percentage using Eq. 2 (Roy and Bhattacharya 2012). C_i and C_e are the initial and equilibrium metal concentrations (mg L^{-1}), m is the mass of adsorbent applied (g) and V is the volume of the solution used (L).

$$q_e = \frac{(C_i - C_e)V}{m} \tag{1}$$

$$\% \text{ Adsorption efficiency} = \frac{(C_i - C_e)}{C_i} \times 100 \tag{2}$$

Adsorption from AMD-contaminated ground and surface water samples

Surface water samples were collected from the Tweelopiespruit, a stream west of Johannesburg into which a disused mineshaft decants mine drainage (26°50′21.67″S, 27°42′57.49″E). Two water samples were collected from the stream at locations approximately 1 and 1.5 km downstream of the decant point. Groundwater was collected from a well in the vicinity of the stream (650 m away from sampling point 1). Water samples were collected in 1-L acid-washed polypropylene bottles and the pH, conductivity and redox activity of water was recorded on site using field meters. Samples were then transported to the laboratory over ice where they were filtered through

0.45-μm filter paper before use in adsorption experiments. The adsorption protocol was similar to that used for simulated wastewater, except that water samples were used without pH adjustment. Thus, 10 mL of water sample was reacted with 10 mL of 3 mg L^{-1} NP suspension for 60 min, filtered and filtrate metal concentrations determined by ICP-OES.

Modeling

Kinetics

Kinetics data were fitted into three kinetics models: the pseudo-first-order model (Eq. 3), pseudo-second-order model (Eq. 4) (Ho and Mckay 2004), and the intraparticle diffusion model (Eq. 5) (Weber and Morris 1963).

$$\log(q_e - q_t) = \log q_e - \left(\frac{k_1}{2.303}\right)t \tag{3}$$

$$\frac{t}{q_t} = \left(\frac{1}{k_2}\right) + \left(\frac{1}{q_e}\right)t \tag{4}$$

$$q_t = I_d + k_p \cdot (t^{0.5}) \tag{5}$$

q_e and q_t are the NP-loading capacities (mg g^{-1}) at equilibrium and at time t, respectively, while k_p is the initial rate of intraparticle diffusion (mg (g^{-1} $s^{-0.5}$)). The equations were plotted as follows: $\log(q_e - q_t)$ versus t for the pseudo-first-order model, t/q_t versus t for the pseudo-second-order model and q_t versus $t^{0.5}$ for the intraparticle diffusion model. Rate constants were determined from the slope (k_1) or intercepts (k_2 and I_d) of respective plots.

Adsorption isotherms

Adsorption isotherms at pH 3 were determined using five different concentrations for each ion. Isotherm data were fitted to the Langmuir and Freundlich models (LeVan and Vermeulen 1981) to determine adsorption capacities and infer the nature of binding of sorbate ions at the sorbent surface. The Langmuir model assumes that adsorption takes place at specific homogenous sites and best describes monolayer adsorption. It is represented in the linear form by Eq. 5 where q_{max} is the maximum concentration of metal ions sorbed per unit weight of NPs (mg g^{-1}), and K_L is the Langmuir constant for the reaction.

The Freundlich model on the other hand, assumes that adsorption takes place on a heterogeneous surface by multi-layer adsorption. Its linear form is as expressed in Eq. 6, where K_F and $1/n$ are constants specific to each reaction. K_F is the relative adsorption capacity of the adsorbent and $1/n$ is related to the adsorption intensity and heterogeneity of the sorbent surface. The more heterogeneous the surface, the closer the $1/n$ value is to 1. $1/n$

values can also be used to infer the nature of adsorption, i.e., values below 1 imply chemisorption and those >1 imply cooperative processes, e.g., adsorption in combination with precipitation (Foo and Hameed 2010).

$$\frac{C_e}{q_e} = \left(\frac{1}{q_{max}}\right) C_e + \left(\frac{1}{K_L q_{max}}\right) \quad (5)$$

$$\log q_e = \left(\frac{1}{n}\right) \log C_e + \log K_F \quad (6)$$

Equations 5 and 6 were plotted as follows: C_e/q_e versus C_e and $\log q_e$ versus $\log C_e$. q_{max} and $1/n$ were determined from the slopes of these plots, while K_L and K_F were determined from the intercepts.

The speciation of metal ions at various pH and in the presence of additional ions was determined using MEDUSA software (KTH Royal Institute of Technology 2004).

Results and discussion

Particle characterisation

Transmission electron micrographs revealed polydisperse polyhedral particles with diameters <100 nm (Fig. 1a). The X-ray diffraction pattern (Fig. 1b) is consistent with the database for this iron phase in the JCPDS file. The
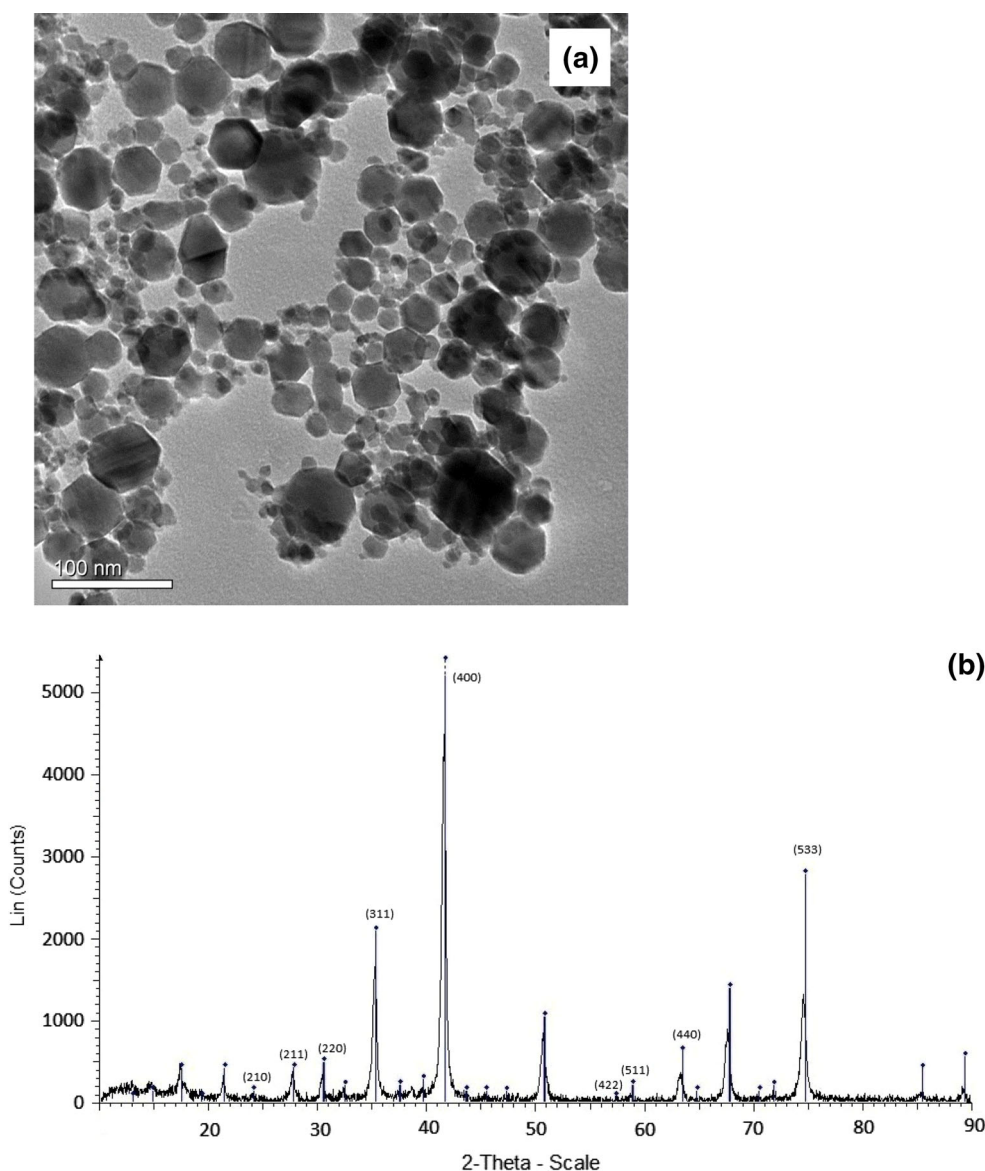

Fig. 1 Transmission electron micrograph (a) and powder X-ray diffractogram (b) of maghemite nanoparticles. PXRD peaks were as indexed according to JCPDS 39-1346

presence of (2 1 0) and (2 1 1) peaks confirms that the adsorbent was indeed maghemite and not magnetite, both of which have similar X-ray diffractograms (Kim et al. 2012). Thus, although all other wide angle peaks, i.e., from (2 2 0) to (5 3 3) are present in both iron oxide phases, magnetite does not have peaks at (2 1 0) and (2 1 1). The presence of these two peaks in the NP sample therefore confirms that it is maghemite. BET measurements indicated that particles were mesoporous (average pore width was 11.3 nm) with a surface area of 40.8 m^2 g^{-1}.

Effect of contact time

Adsorption was quantified at the following time intervals: 5, 10, 15, 30, 45, 60, 300, 600, 900, 1,800, 2,700 and 3,600 s. Adsorption of all three metal ions was rapid and reactions attained equilibrium within 30 min (Fig. 2). At equilibrium 56 % of Cu, 53 % of Mn and 49 % of U were adsorbed from solutions at pH 3. Similar rapidity of reaction rates was also reported by Chang and Chen (2005) and Banerjee and Chen (2007).

Reaction kinetics were best described by the pseudo-second-order model (Table 1), implying that the binding of metal ions to the maghemite surface was by chemisorption (Ho and Mckay 2004). Further, the fit of data to the intraparticle diffusion model was poor ($R^2 \leq 0.11$). Diffusion to sorption sites within pores was therefore not the rate-limiting step in the adsorption process. This can be
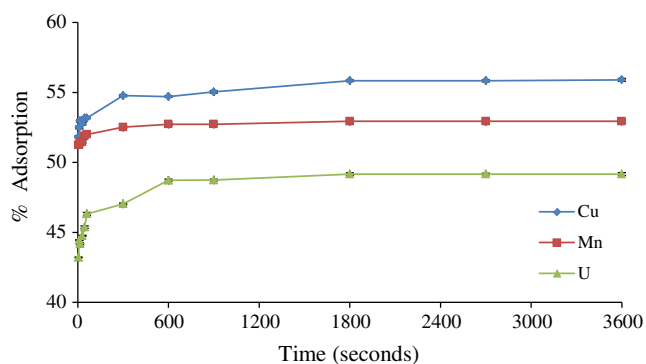

Fig. 2 The kinetics of Cu, Mn and U adsorption to maghemite NPs (±SD) at pH 3 (NP concentration 3 mg L^{-1})

explained by the fact that with NP pore diameters of 11.3 nm, hydrated Cu (radius = 0.419 nm), Mn (radius = 0.438 nm) and U (radius = 1.08 nm) ions should have un-impeded access and movement within NP pores (Persson 2010).

Notably, the adsorption rate was highest for Mn. This was despite the higher initial concentrations hence higher mass transfer drives for Cu and U, as well as the fact that Cu is more electronegative than Mn. Madden et al. (2006) hypothesized that NPs differentially bind metal ions based on their structural configuration. Thus, in their study, adsorption of Cu to hematite increased with decreasing hematite NP size because of the higher incidence, in smaller particles, of sites that stabilized the Jahn–Teller distorted octahedron of Cu. Similarly, the configuration of sorption sites on the maghemite surface may favor the perfect octahedron of Mn relative to the Jahn–Teller distorted Cu, hence the higher adsorption rate of the former. With respect to U, the large ionic size may be responsible for the low-binding rate.

Effects of Mn^{2+} and SO$_4^{2-}$ ions

The adsorption of all three metal ions at pH 3 was enhanced in the presence of Mn^{2+} (Fig. 3a) and SO$_4^{2-}$ ions (Fig. 3b). U adsorption was largely similar in both equimolar and 1:2 U/Mn molar solutions, i.e., adsorption increased by 10 and 11 %, respectively (Fig. 3a). In contrast, Cu sorption increased by 15 % in 1:1 Cu-to-Mn solutions and by only 7 % in 1:2 Cu-to-Mn solutions. Cu adsorption was therefore inhibited by higher Mn concentrations. This leads to the hypothesis that Cu and Mn ions sorb to similar sites on the adsorbent surface (Benjamin and Leckie 1981), resulting in competition in mixed solutions. The high Mn concentrations in AMD may therefore, inhibit adsorption of Cu to maghemite NPs at low pH.

Increases in the presence of sulphate ions were largely similar in both 1:1 and 1:2 metal-to-sulphate solutions (Fig. 3b). The greatest effect of sulphate was on U and Mn, while the least was on Cu. In the treatment of AMD, therefore, the presence of sulphate is likely to have synergistic effects and improve removal efficiency of NPs.

Table 1 Adsorption rate constants and coefficients of correlation (R^2) for kinetics models fitted to adsorption data

Metal	Initial concentration (mg L^{-1})	Pseudo-second order model			Pseudo-first order model			Intraparticle diffusion model
		k_2 (g mg^{-1} s^{-1})	q_e (mg g^{-1})	R^2	k_1 (sec^{-1})	q_e (mg g^{-1})	R^2	R^2
Cu	14.99	0.01	27.93	1	0.002	1.58	0.95	0.14
Mn	9.55	0.04	16.81	1	0.001	2.55	0.78	0.11
U	42.18	0.002	69.44	0.99	0.004	5.57	0.87	0.16

Adsorption at pH 3, adsorbent concentration = 3 mg L^{-1}; volume of adsorbent solution used = 10 mL; volume of metal solution = 10 mL
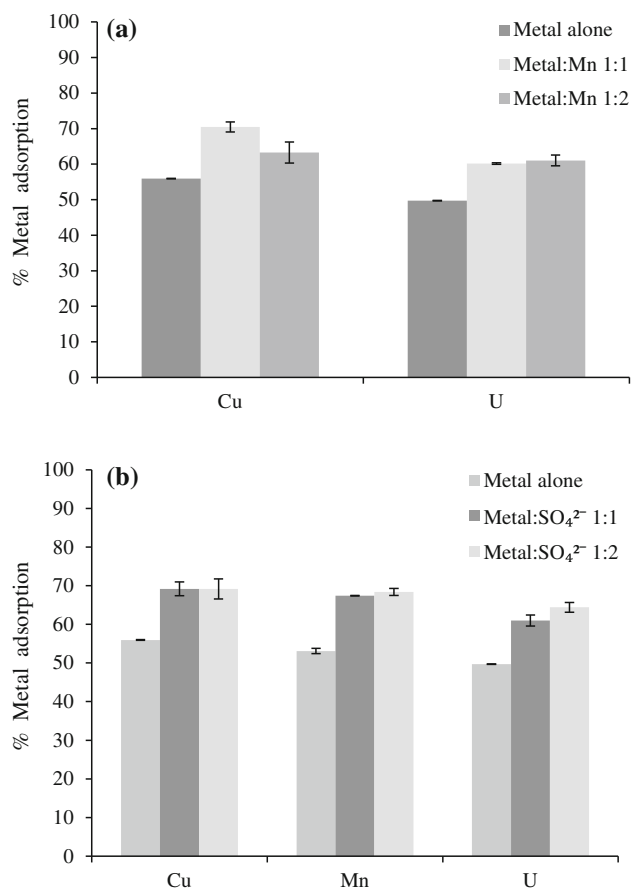
Fig. 3 **a** The effect of manganese ions on adsorption of Cu and U by maghemite NPs (±SD). **b** The effect of sulphate ions on adsorption of Cu, Mn and U by maghemite NPs (±SD)

Mechanisms of adsorption enhancement

Adsorption enhancement in the presence of Mn was likely due to a greater diffusion drive for mass transfer to the adsorbent surface (Ho and Mckay 2004). Driving forces for diffusion of ions towards the adsorbent surface are greater at high ion concentrations, hence increased adsorption.

Enhanced adsorption in the presence of sulphates (and anions like phosphate and arsenate) has been reported previously. Ali and Dzombak (1996), for example, found that the adsorption of Cu at low pH was enhanced in the presence of sulphate. Similarly, arsenate enhanced the sorption of Zn to goethite while phosphate and sulphate ions enhanced sorption of Pb to goethite and boehmite (Weesner and Bleam 1998) and Cd to goethite (Collins et al. 1999).

A number of mechanisms have been proposed to explain these observations. The first is that anions lower the energy barrier for the approach of cations to the adsorbent surface by forming complexes in solution (James and Healy 1972a). Thus, the formation of uncharged complexes such as $CuSO_4$, $MnSO_4$ and UO_2SO_4 can increase adsorption

because these complexes experience less repulsion from the maghemite surface than do charged ions. Alternatively, anions may increase adsorption by altering the electrical properties of the adsorbent surface (Benjamin and Leckie 1982). The adsorption of sulphate to maghemite reduces Coulombic repulsions, making the interaction between maghemite sorption sites and cations more favorable. The formation of ternary surface complexes was also suggested by the modeling studies of Ali and Dzombak (1996) and Swedlund and Webster (2001). However, EXAFS (extended x-ray absorption fine structure) and ATR-FTIR (attenuated total reflectance–fourier transform infrared) spectroscopic data by Collins et al. (1999) and Beattie et al. (2008) found no evidence of such structures.

Nonetheless, these and other spectroscopic techniques [EXAFS and X-ray Absorption Spectroscopy (XAS)] resolved U and Cu binding to iron oxides (goethite, schwertmannite and ferrihydrite) as involving the formation of inner sphere complexes (Moyes et al. 2000; Walter et al. 2003). While U complexes may be mononuclear bidentate, binuclear bidentate or mononuclear monodentate, those of Cu are bidentate ($[\equiv FeOH_2)Cu(OH_2)^0]$) or tridentate ($[\equiv Fe_3O(OH_2)Cu_2(OH)_3^0]$) (Peacock and Sherman 2004). With respect to Mn, although we could find no spectroscopic evidence, its adsorption to iron oxides likely also involves formation of inner sphere complexes. This is because adsorption at pH 3, where both maghemite and Mn are positively charged, likely involves specific and not electrostatic interactions (James and Healy 1972b).

Effect of initial metal concentrations

Although percent differences are relatively imperceptible (especially for Cu and Mn), it is clear from Fig. 4a–c that NP loading (q_e) increased with increasing metal concentrations. These increases can be explained by the greater driving force for mass transfer as ion concentrations in solution increase (Ho and Mckay 2004).

As shown in Table 2, the better fit of adsorption data for all three metal ions was given by the Freundlich model, implying that adsorption was to a heterogeneous surface. The $1/n$ values show that adsorption of Cu and Mn was by chemisorption. In addition, the K_F values for these two ions indicate that affinity for sorption sites under the experimental conditions was greater for Mn than Cu. Nevertheless, calculated maximum adsorption capacities for the two metal ions varied little. The removal of U on the other hand, was by cooperative processes, based on the $1/n$ value that was >1. Adsorbent capacity for this ion was, however, lower than that of Cu and Mn. Indeed, a comparison of the adsorption capacity of maghemite NPs and a few other adsorbents is presented in Table 3. From these data, it is clear that at low pH, maghemite NPs have a higher

adsorption capacity for Cu than hematite NPs (Grover et al. 2012). Their capacity for Mn is also almost equal to that of activated carbon (Mohan et al. 2001), but lower than that of reduced graphene oxide with respect to U adsorption (Li et al. 2012). The higher adsorption capacity for maghemite NPs reported by Hu et al. (2006) was due to the larger surface area of the NPs in that study (198 $m^2 g^{-1}$ vs. 40 $m^2 g^{-1}$ for particles in this study), along with the higher pH at which adsorption was conducted. Similarly, the high adsorption efficiency reported by Roy and Bhattacharya (2012) is because of the higher surface area of their nanotubes (111.11 $m^2 g^{-1}$).

Effect of adsorbent concentration

Adsorbed metal concentrations fluctuated, albeit slightly, with increasing NP concentrations. Cu adsorption went from 52 to 56 % and then 51 % as NP concentrations increased from 1 to 3 and 10 mg L^{-1} (Fig. 5). Mn adsorption went from 50 to 53 % and 52 %, while U adsorption went from 48 to 50 % and 48 % at 1, 3 and 10 mg L^{-1} NP concentrations. The optimal NP concentration was therefore 3 mg L^{-1} in all cases, but differences were small. Decreases in adsorption at 10 mg L^{-1} NP concentrations were likely due to NP agglomeration which increases with, among other things, NP concentrations (He et al. 2008). Particle agglomeration reduces the access of metal ions to sorption sites located in the interior of particles and agglomerates. This, in turn, reduces metal removal efficiency. Care must therefore be exercised in determining the NP concentrations to be used in remediation systems as higher NP concentrations do not always give greater adsorption yields.

Effect of pH

The influence of pH on adsorption was studied at pH 3, 5, 7 and 9. As shown in Fig. 6, removal of all three ions increased with pH. The increase between pH 3 and 9 was least for Mn (9 %) and highest for Cu (31 %). U removal increased by 27 % between pH 3 and 9, with the greatest increase occurring between pH 5 and 7. At this pH range, a hydrolysis product of uranium, schoepite [$(UO_2)_8O_2(OH)_{12}\cdot12H_2O$] is formed hence the increase in adsorption (Tutu 2006). However, because experiments did not exclude CO_2, not all uranium precipitated as schoepite due to the formation of uranyl carbonates and hydrogen carbonates (Waite et al. 1994; Wazne et al. 2006). Indeed, adsorption did not attain maximal efficiencies likely due to the formation of these non-adsorbing species.

Changes in adsorption of ions may be due to any of the following three effects, acting most often, simultaneously: (1) reduced competition from H^+ ions, (2) changes in the adsorbent surface charge and (3) hydrolysis (James and
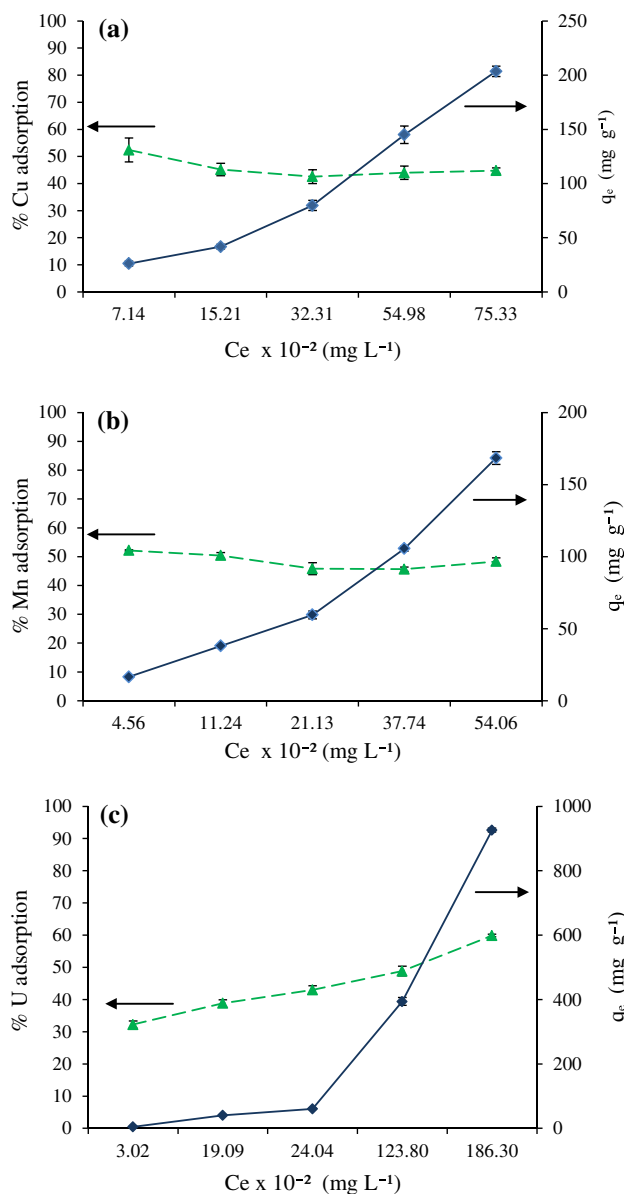

Fig. 4 Adsorption isotherms and percent adsorption efficiencies of Cu (**a**), Mn (**b**) and U (**c**) (±SD)
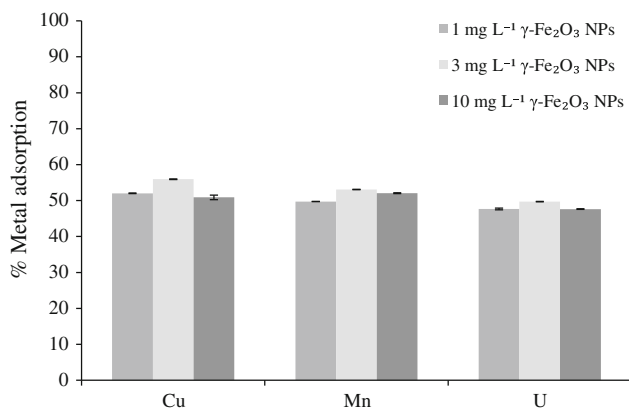
Table 2 Langmuir and Freundlich isotherm parameters determined for the adsorption of Cu, Mn and U to maghemite NPs

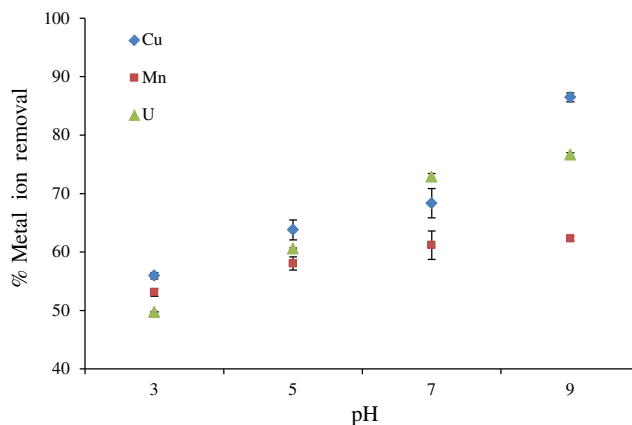| Metal	Freundlich isotherm			Langmuir isotherm		
	R^2	K_F (mg g^{-1})	$1/n$	R^2	q_{max} (mg g^{-1})	K_L
Cu	0.96	4.35	0.83	0.31	108.7	0.03
Mn	0.99	4.03	0.91	0.32	208.3	0.02
U	0.99	1.13	1.25	0.94	20.3	0.07

Adsorption at pH 3, adsorbent concentration = 3 mg L^{-1}; volume of adsorbent solution used = 10 mL; volume of metal solution = 10 mL; equilibration time = 60 min

Table 3 A comparison of the adsorption capacities of maghemite NPs and other adsorbents for Cu, Mn and U

Adsorbent	Metal	Solution pH	Adsorption capacity (mg g^{-1})	References
Maghemite NPs	Cu	3	4.35	This study
Maghemite NPs		6.5	27.7	Hu et al. (2006)
Maghemite nanotubes		6	111.11	Roy and Bhattacharya (2012)
Hematite NPs		4	2.92	Grover et al. (2012)
Magnetite NPs		6	17.6	Banerjee and Chen (2007)
Maghemite NPs	Mn	3	4.03	This study
Activated carbon (wood)		6	4.16	Mohan and Chander (2001)
Activated carbon (coconut shell)		6	16.42	Mohan and Chander (2001)
Lignite		3.5	28.54	Mohan and Chander (2006)
Maghemite NPs	U	3.3	1.13	This study
Magnetite NPs		8.1	5	Das et al. (2010)
Reduced graphene sheets		4	47	Li et al. (2012)

Fig. 6 The effect of pH on adsorption of Cu, Mn and U to maghemite NPs ($\pm$SD). Initial concentrations: 14.99 mg L^{-1} for Cu, 9.52 mg L^{-1} for Mn and 42.18 mg L^{-1} for U; NP concentration: 3 mg L^{-1})

moieties are increasingly deprotonated (Eqs. 7, 8) making the approach of cations to the maghemite surface, and subsequently adsorption, more favorable.

$$\equiv FeOH_2^+ \rightarrow \equiv FeOH + H^+ \tag{7}$$

$$\equiv FeOH \rightarrow \equiv FeO^- + H^+ \tag{8}$$
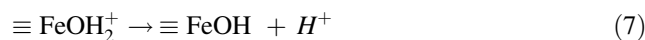
The third factor, hydrolysis, increases adsorption through the formation of more adsorbable species as postulated by James and Healy (1972a). Thus, adsorption of Cu and U increased at higher pH, due to the formation of species such as CuOH$^+$, Cu(OH)$_2$, (UO$_2$)$_2$(OH)$_2^{2+}$, and insoluble precipitates. Speciation modeling showed that insoluble UO$_2$(OH)$_2\cdot$H$_2$O and CuO form were the dominant species in solutions higher than pH 5 and 5.6, respectively. This explains why the largest increase in U sorption is seen between pH 5 and 7 as well as why Cu removal increased at pH 7 and 9. Mn, on the other hand, does not hydrolyze in the test pH range; hence, the minimal change in adsorption. In fact, Mn adsorption likely increased only due to decreased competition from H$^+$ ions, and changes on the adsorbent surface.

The pH$_{PZC}$ of particles also has an effect on the nature of adsorption. As particle surfaces are positively charged below the pH$_{PZC}$, cation adsorption in this pH region likely involves specific interactions. In contrast, adsorption above the pH$_{PZC}$, where cations and adsorbent surfaces are oppositely charged, involves electrostatic forces. For maghemite, therefore, adsorption across the test pH range was by both specific (ion exchange) and electrostatic interactions.

Another effect that solution pH has on adsorption relates to NP agglomeration. As solution pH approaches the pH$_{PZC}$ of NPs, agglomeration increases due to the decrease in

Fig. 5 The effect of adsorbent concentration on adsorption of Cu, Mn and U to maghemite NPs ($\pm$SD)

Healy 1972b). As solution pH increases, the concentration of H$^+$ ions decreases, resulting in less competition between them and cations for sorption sites. pH-related changes to the adsorbent surface also affect the adsorption of cations. Maghemite, with a pH$_{PZC}$ of 6.3–6.9 (Vayssieres 2009) is positively charged below pH 6.3–6.9 but becomes increasingly negatively charged as pH increases. Thus, at low pH, $\equiv$FeO$_2^+$ groups dominate the maghemite surface and repulse cations. As pH increases, however, these

Table 4 Physical and chemical characteristics of AMD-contaminated surface water (SW) and groundwater (GW) used in application studies

Sample	pH	Conductivity (mS cm^{-1})	Redox potential (mV)	[Cu]$_{tot}$, mg L^{-1} (SD)	[Mn]$_{tot}$, mg L^{-1} (SD)	[U]$_{tot}$, mg L^{-1} (SD)
SW1	3.13	3.52	209.0	1.44 (0.003)	49.74 (0.002)	b.d
SW2	2.79	3.87	227.7	1.22 (0.046)	16.48 (0.006)	b.d
GW	5.62	2.76	6.9	0.24 (0.001)	15.00 (0.140)	b.d

[ ]$_{tot}$ Total concentration of all species, *b.d* concentration below ICP-OES detection limit
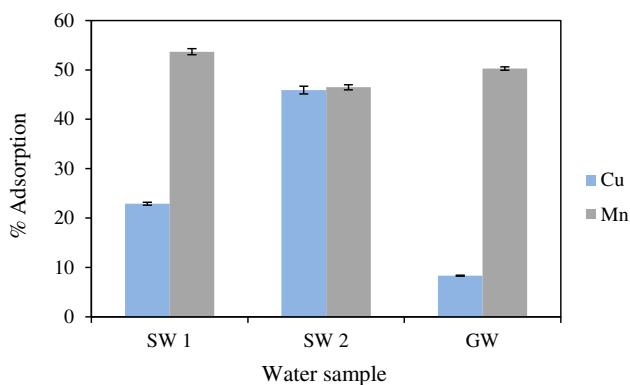
Fig. 7 Removal efficiencies of Cu and Mn from contaminated surface and groundwater by maghemite NPs. U concentrations in both surface and groundwater samples were below detection limits for ICP-OES

repulsive surface charges (He et al. 2008). This, as discussed above ("Effect of adsorbent concentration"), reduces access to sorption sites and decreases adsorption. Although difficult to determine separately from the effects of all other factors mentioned, it is still worth bearing in mind during the determination of operational parameters, that adsorption may decline as solution pH approaches NP pH$_{PZC}$.

Application studies

Removal of Cu, Mn and U by maghemite NPs was then tested in AMD-contaminated water. Two surface water samples (SW1 and SW2) and one ground water sample (GW) were used. The physical and chemical characteristics of contaminated water samples are presented in Table 4. U concentrations in all three water samples were below ICP-OES detection limits, hence removal could not be quantified.

The results of adsorption experiments are presented in Fig. 7. Of the three water samples, Cu was most efficiently removed from SW2 while Mn was more efficiently adsorbed from SW1. Adsorption of both ions in SW2 was almost equal. Importantly, these data confirm our earlier hypothesis that high Mn concentrations inhibit Cu sorption to maghemite. Thus, although Cu concentrations in SW1

and SW2 were almost similar (Table 4), Cu adsorption from SW2 was double that of SW1, i.e., 46 versus 23 %. This difference may be ascribed to the ratio of Cu:Mn in the two water samples which was 1:35 in SW1 but only 1:14 in SW2. Thus, the much higher Mn concentrations in SW1 limited Cu adsorption from that water sample. The low Cu removal from ground water where the Cu:Mn ratio was 1:63 also corroborates this hypothesis. Nonetheless, these experiments confirm that maghemite NPs can be applied for the remediation of actual AMD-contaminated waters.

Conclusions

Metal contamination of water resources is a growing environmental problem in many mining regions. In addition, increasing pressure on water resources means that demand for technologies for the remediation of contaminated waters will only increase. In this work, the adsorption of Cu, Mn and U ions by maghemite NPs was investigated with the aim of determining NP applicability for the remediation of AMD-contaminated waters. The results show that adsorption at pH 3.3 (±0.2) was rapid and adsorption efficiencies were 56, 53 and 49 % for Cu, Mn and U, respectively.

Adsorption increased in the presence of manganese and sulphate ions, but higher manganese concentrations inhibited Cu sorption. The presence of sulphates, at concentrations similar to those tested here, is therefore likely to increase adsorption of Cu, Mn and U from AMD while manganese may have antagonistic effects on Cu removal by maghemite.

Adsorption was also enhanced at higher pH with removal efficiencies increasing to 86, 62 and 77 % at pH 9 for Cu, Mn and U, respectively. Maghemite NPs can therefore be applied for the removal of Cu, Mn and U from mine drainage both at low and high pH.

Increasing NP concentrations did not, however, always increase adsorbed metal concentrations. Adsorption increased as NP concentration increased from 1 to 3 mg L^{-1} but decreased at 10 mg L^{-1} NP concentrations, likely due to increased agglomeration at higher NP concentrations.

Importantly, work with actual AMD-contaminated surface and groundwater samples confirms that maghemite NPs can indeed be applied for the removal of Cu and Mn from field samples. Although U removal could not be determined due to concentrations below instrument detection capacity, the capability of its removal by maghemite was already established in simulated wastewater. These NPs therefore offer, particularly for Mn, a remediation alternative that does not require pH adjustment or the copious amounts of lime required to achieve this. Low pH waters can, therefore, be directly treated and adjustments to neutral pH would require less time.

The work presented here suggests that metal removal could be optimized based on a combination of pH adjustment and NP concentrations for the treatment of AMD and this is potentially viable for further research. Ongoing work involves quantifying desorption for purposes of re-using NPs in multiple cycles and functionalization of NP surfaces to improve adsorption efficiency.

References

Afkhami A, Norooz-Asl R (2009) Removal, preconcentration and determination of Mo(VI) from water and wastewater samples using maghemite nanoparticles. Colloids Surf A Physicochem Eng Asp 346:52–57. doi:10.1016/j.colsurfa.2009.05.024

Ali MA, Dzombak DA (1996) Interactions of copper, organic acids, and sulfate in goethite suspensions. Geochim Cosmochim Acta 60:5045–5053. doi:10.1016/S0016-7037(96)00311-0

Banerjee SS, Chen D-H (2007) Fast removal of copper ions by gum arabic modified magnetic nano-adsorbent. J Hazard Mater 147:792–799. doi:10.1016/j.jhazmat.2007.01.079

Beattie DA, Chapelet JK, Gräfe M et al (2008) In situ ATR-FTIR studies of SO_4 adsorption on goethite in the presence of copper ions. Environ Sci Technol 42:9191–9196. doi:10.1021/es801767b

Benjamin MM, Leckie JO (1981) Competitive adsorption of Cd, Cu, Zn, and Pb on amorphous iron oxyhydroxide. J Colloid Interface Sci 83:410–419. doi:10.1016/0021-9797(81)90337-4

Benjamin MM, Leckie J (1982) Effects of complexation by Cl, SO_4 and S_2O_3 on adsorption behaviour of Cd on oxide surfaces. Environ Sci Technol 16:162–170. doi:10.1021/es00097a008

Chang Y-C, Chen D-H (2005) Preparation and adsorption properties of monodisperse chitosan-bound Fe_3O_4 magnetic nanoparticles for removal of Cu(II) ions. J Colloid Interface Sci 283:446–451. doi:10.1016/j.jcis.2004.09.010

Collins CR, Vala RK, Sherman DM (1999) Effect of inorganic and organic ligands on the mechanism of cadmium sorption to goethite. Geochim Cosmochim Acta 63:2989–3002. doi:10.1016/S0016-7037(99)00226-4

Das D, Sureshkumar MK, Koley S, et al (2010) Sorption of uranium on magnetite nanoparticles. J Radioanal Nucl Chem 285:447–454. doi:10.1007/s10967-010-0627-0

Foo KY, Hameed BH (2010) Insights into the modeling of adsorption isotherm systems. Chem Eng J 156:2–10. doi:10.1016/j.cej.2009.09.013

Franklin NM, Stauber JL, Markich SJ, Lim RP (2000) pH-dependent toxicity of copper and uranium to a tropical freshwater alga (*Chlorella* sp.). Aquat Toxicol 48:275–289. doi:10.1016/S0166-445X(99)00042-9

Fu F, Wang Q (2011) Removal of heavy metal ions from wastewaters: a review. J Environ Manage 92:407–418. doi:10.1016/j.jenvman.2010.11.011

Grover VA, Hu J, Engates KE, Shipley HJ (2012) Adsorption and desorption of bivalent metals to hematite nanoparticles. Environ Toxicol Chem 31:86–92. doi:10.1002/etc.712

He YT, Wan J, Tokunaga T (2008) Kinetic stability of hematite nanoparticles: the effect of particle sizes. J Nanoparticle Res 10:321–332. doi:10.1007/s11051-007-9255-1

Ho YS, Mckay G (2004) Sorption of copper(II) from aqueous solution by peat. Water Air Soil Pollut 158:77–97. doi:10.1023/B:WATE.0000044830.63767.a3

Hu J, Chen G, Lo IMC (2006) Selective removal of heavy metals from industrial wastewater using maghemite nanoparticle: performance and mechanisms. J Environ Eng 132:709–715. doi:10.1061/(ASCE)0733-9372(2006)132:7(709)

James R, Healy T (1972a) Adsorption of hydrolyzable ions at the oxide-water interface. III. A thermodynamic model of adsorption. J Colloid Interface Sci 40:65–81. doi:10.1016/0021-9797(72)90174-9

James R, Healy T (1972b) Adsorption of hydrolyzable ions at the oxide-water interface. I. Co(II) adsorption on SiO_2 and TiO_2 as model systems. J Colloid Interface Sci 40:42–52. doi:10.1016/0021-9797(72)90174-9

Jiang W, Pelaez M, Dionysiou DD et al (2013) Chromium(VI) removal by maghemite nanoparticles. Chem Eng J 222:527–533. doi:10.1016/j.cej.2013.02.049

Jordan N, Ritter A, Foerstendorf H et al (2013) Adsorption mechanism of selenium(VI) onto maghemite. Geochim Cosmochim Acta 103:63–75. doi:10.1016/j.gca.2012.09.048

Khajeh M, Laurent S, Dastafkan K (2013) Nanoadsorbents: classification, preparation, and applications (with emphasis on aqueous media). Chem Rev 113:7728–7768

Kim W, Suh C-Y, Cho S-W et al (2012) A new method for the identification and quantification of magnetite—maghemite mixture using conventional X-ray diffraction technique. Talanta 94:348–352. doi:10.1016/j.talanta.2012.03.001

KTH Royal Institute of Technology (2004) HYDRA/MEDUSA

Kurniawan TA, Chan GYS, Lo W-H, Babel S (2006) Physico-chemical treatment techniques for wastewater laden with heavy metals. Chem Eng J 118:83–98. doi:10.1016/j.cej.2006.01.015

LeVan MD, Vermeulen T (1981) Binary Langmuir and Freundlich isotherms for ideal adsorbed solutions. J Phys Chem 85:3247–3250. doi:10.1021/j150622a009

Li Z, Chen F, Yuan L et al (2012) Uranium(VI) adsorption on graphene oxide nanosheets from aqueous solutions. Chem Eng J 210:539–546. doi:10.1016/j.cej.2012.09.030

Madden AS, Hochella MF, Luxton TP (2006) Insights for size-dependent reactivity of hematite nanomineral surfaces through Cu^{2+} sorption. Geochim Cosmochim Acta 70:4095–4104. doi:10.1016/j.gca.2006.06.1366

Madrakian T, Afkhami A, Rahimi M (2011) Removal, preconcentration and spectrophotometric determination of U(VI) from water samples using modified maghemite nanoparticles. J Radioanal Nucl Chem 292:597–602. doi:10.1007/s10967-011-1453-8

Mohan D, Chander S (2001) Single component and multi-component adsorption of metal ions by activated carbons. Colloids Surf A Physicochem Eng Asp 177:183–196. doi:10.1016/S0927-7757(00)00670-1

Mohan D, Chander S (2006) Single, binary and multicomponent sorption of iron and manganese on lignite. J Colloid Interface Sci 299:76–87. doi:10.1016/j.jcis.2006.02.010

Mohan D, Gupta VK, Srivastava SK, Chander S (2001) Kinetics of mercury adsorption from wastewater using activated carbon derived from fertilizer waste. Coloids Surf A Physicochem Eng Asp 177:169–181

Moyes LN, Parkman RH, Charnock JM et al (2000) Uranium uptake from aqueous solution by interaction with goethite, lepidocrocite, muscovite, and mackinawite: an X-ray absorption spectroscopy study. Environ Sci Technol 34:1062–1068. doi:10.1021/es990703k

Naicker K, Cukrowska E, McCarthy TS (2003) Acid mine drainage arising from gold mining activity in Johannesburg, South Africa and environs. Environ Pollut 122:29–40. doi:10.1016/S0269-7491(02)00281-6

Peacock CL, Sherman DM (2004) Copper(II) sorption onto goethite, hematite and lepidocrocite: a surface complexation model based on ab initio molecular geometries and EXAFS spectroscopy. Geochim Cosmochim Acta 68:2623–2637. doi:10.1016/j.gca.2003.11.030

Persson I (2010) Hydrated metal ions in aqueous solution: how regular are their structures? Pure Appl Chem 82:1901–1917. doi:10.1351/PAC-CON-09-10-22

Roy A, Bhattacharya J (2012) Removal of Cu(II), Zn(II) and Pb(II) from water using microwave-assisted synthesized maghemite nanotubes. Chem Eng J 211–212:493–500. doi:10.1016/j.cej.2012.09.097

Saad DM, Cukrowska EM, Tutu H (2013) Selective removal of mercury from aqueous solutions using thiolated cross-linked polyethylenimine. Appl Water Sci 3:527–534. doi:10.1007/s13201-013-0100-7

Schemel LE, Kimball BA, Bencala KE (2000) Colloid formation and metal transport through two mixing zones affected by acid mine drainage near Silverton, Colorado. Appl Geochem 15:1003–1018. doi:10.1016/S0883-2927(99)00104-3

Swedlund P, Webster J (2001) Cu and Zn ternary surface complex formation with SO$_4$ on ferrihydrite and schwertmannite. Appl Geochem 16:503–511. doi:10.1016/S0883-2927(00)00044-5

Toens PD, Standler W, Wullschleger NJ (1998) The association of groundwater chemistry and geology with atypical lymphocytes (as a biological indicator) in the Pofadder area. North Western Cape, South Africa 64

Tutu H (2006) Determination and geochemical modelling of the dispersal of uranium in gold-mine polluted land on the Witwatersrand Basin. University of the Witwatersrand

Tutu H, McCarthy TS, Cukrowska E (2008) The chemical characteristics of acid mine drainage with particular reference to sources, distribution and remediation: the Witwatersrand Basin, South Africa as a case study. Appl Geochem 23:3666–3684. doi:10.1016/j.apgeochem.2008.09.002

Tuutijärvi T, Lu J, Sillanpää M, Chen G (2009) As(V) adsorption on maghemite nanoparticles. J Hazard Mater 166:1415–1420. doi:10.1016/j.jhazmat.2008.12.069

Vayssieres L (2009) On the effect of nanoparticle size on water-oxide interfacial chemistry. J Phys Chem C 113:4733–4736. doi:10.1021/jp810721f

Waite TD, Davis JA, Payne TE et al (1994) Uranium(VI) adsorption to ferrihydrite: application of a surface complexation model. Geochim Cosmochim Acta 58:5465–5478. doi:10.1016/0016-7037(94)90243-7

Walter M, Arnold T, Reich T, Bernhard G (2003) Sorption of uranium(VI) onto ferric oxides in sulfate-rich acid waters. Environ Sci Technol 37:2898–2904

Waychunas GA, Zhang H (2008) Structure, chemistry, and properties of mineral nanoparticles. Elements 4:381–388. doi:10.2113/gselements.4.6.381

Wazne M, Meng X, Korfiatis GP et al (2006) Carbonate effects on hexavalent uranium removal from water by nanocrystalline titanium dioxide. J Hazard Mater 166:1415–1420. doi:10.1016/j.jhazmat.2005.11.010

Weber JW, Morris JC (1963) Kinetics of adsorption on carbon from solutions. J Sanit Eng Div Am Soc Civ Eng 89:31–60

Weesner FJ, Bleam WF (1998) Binding characteristics of Pb^{2+} on anion-modified and pristine hydrous oxide surfaces studied by electrophoretic mobility and X-ray absorption spectroscopy. J Colloid Interface Sci 205:380–389. doi:10.1006/jcis.1998.5629

WHO (2011) WHO guidelines for drinking-water quality. WHO Chron 38:564

Winde F (2010) Uranium pollution of the Wonderfonteinspruit, 1997–2008. Part 2: uranium in water—concentrations, loads and associated risks. Water SA 36:257–278